2 mil

NASA TECHNICAL MEMORANDUM

NASA TM X- 62,338

NASA TM X- 62,338

NUMERICAL SOLUTION OF THE TIME–DEPENDENT COMPRESSIBLE NAVIER–STOKES EQUATIONS IN INLET REGIONS

L. E. Olson

U. S. Army Air Mobility R&D Laboratory
Moffett Field, Calif. 94035

P. R. McGowan

Computer Sciences Corporation
Mountain View, Calif. 94043

R. W. MacCormack

Ames Research Center
Moffett Field, Calif. 94035

March 1974

Numerical solution of the time-dependent compressible Navier-Stokes equations in inlet regions

By L. E. OLSON

United States Army Air Mobility Research and Development Laboratory,

Ames Research Center

P. R. McGOWAN

Computer Sciences Corporation, Field Services Division, Mountain View,

California 94043

AND R. W. MacCORMACK

Ames Research Center, National Aeronautics and Space Administration,

Moffett Field, California 94035

This paper presents the results of a study to determine the effects of compressibility on the viscous flow through channels that have straight, parallel walls. Two channel configurations are considered, the flow between two semi-infinite flat plates with uniform flow prescribed at the inlet plane and a cascade of semi-infinite flat plates with uniform flow introduced upstream. The flow field is modeled by using the time-dependent, compressible Navier-Stokes equations. Time-dependent solutions are obtained by using an explicit finite-difference technique which advances the pressure on near-field subsonic boundaries such that accurate steady-state solutions are obtained. The steady-state results at Reynolds numbers 20 and 150 are presented for Mach numbers between 0.09 and 0.36 and compared with the incompressible solutions of previous studies.

1. Introduction

The flow in the inlet region of a straight channel brings with it many of the features typical of viscous flow, and thus provides an interesting test case for developing new analytical and numerical methods to be used in the study of more practical flows. As a result, there is an extensive list of references which address this problem, beginning with the original work of Boussinesq (1891). Analytical studies by Schlichting (1960), Blankenship and Chung (1967), Van Dyke (1970), Wilson (1971), and Kapila, Ludford, and Olunloyo (1970) represent some of the more current publications where asymptotic solutions for large Reynolds number have been constructed. With the exception of the work by Blankenship and Cheng, all are restricted to incompressible flow. Additional investigators have approached the problem numerically. Among those using the incompressible Navier-Stokes equations are Gillis and Brandt (1964), Wang and Longwell (1964), Freidman, Gillis, and Liron (1968), Gosman (1969), and McDonald, Denny, Mills (1972), and Morihara and Cheng (1973). Taylor and Ndefo (1970) solve the time-dependent incompressible equations of motion. These works, and others, form the basis for a fundamental understanding of incompressible inlet flows. To the authors' knowledge, however, no solutions have been obtained for this type of problem using the unsteady, compressible Navier-Stokes equations.

Three basic models are generally considered in the literature: uniform flow into a straight channel, irrotational flow into a straight channel, and a cascade of semi-infinite flat plates immersed in a uniform flow. The infinite cascade most accurately simulates a physically realizable flow, and is considered in this report, as is the uniform entry flow which Van Dyke (1970) suggests may be attainable through the use of a variable porosity mesh. In flows such as these, it is important that particular attention be given to the

boundary conditions on near-field permeable boundaries; that is, boundaries where the flow either enters or leaves the computational region. This situation is relieved to some degree for incompressible flow, where it is possible to eliminate the pressure from the governing equations by a transformation into the stream function-vorticity plane. The resulting equations, when coupled with the appropriate boundary conditions, can then be used to solve for the velocity field without reference to any boundary condition on the pressure. The pressure field can then be computed by integrating the momentum equations with a priori knowledge of the pressure required at only one point in the flow field.

For the compressible case, it is not possible to uncouple the pressure and, as a result, a boundary condition on this variable is also required. In addition, with unsteady calculations the pressure conditions become a function of time, which must be generated as part of the solution. In the present paper, a boundary condition which permits the pressure on an upstream subsonic inflow boundary to become a function of time is combined with the explicit finite-difference technique of MacCormack (1970) to solve the compressible time-dependent Navier-Stokes equations. This boundary condition does not require a priori knowledge of the static pressure on the inflow boundary, although the analysis does assume that boundary conditions on the two velocity components and density at this location are specified. Steady-state solutions with low subsonic Mach numbers are compared with the incompressible results of previous authors. Solutions at Mach numbers where compressibility effects become important are also presented.

2. Differential equations and numerical method

The Navier-Stokes equations, in two dimensions, for a time-dependent compressible flow may be written in vector form as

$$\frac{\partial U}{\partial t} + \frac{\partial F}{\partial x} + \frac{\partial G}{\partial y} = 0, \tag{1}$$

where

$$U = \begin{bmatrix} \rho \\ \rho u \\ \rho v \\ e \end{bmatrix};$$

$$F = \begin{bmatrix} \rho u \\ \rho u^2 + \sigma_x \\ \rho uv + \tau_{xy} \\ (e + \sigma_x)u + \tau_{yx}v - k\frac{\partial T}{\partial y} \end{bmatrix},$$

$$G = \begin{bmatrix} \rho v \\ \rho uv + \tau_{xy} \\ \rho v^2 + \sigma_y \\ (e + \sigma_y)v + \tau_{xy}u - k\frac{\partial T}{\partial y} \end{bmatrix},$$

$$\sigma_x = p - \lambda\left[\frac{\partial u}{\partial x} + \frac{\partial v}{\partial y}\right] - 2\mu\frac{\partial u}{\partial x},$$

$$\tau_{xy} = \tau_{yx} = -\mu\left[\frac{\partial u}{\partial y} + \frac{\partial v}{\partial x}\right],$$

and

$$\sigma_y = p - \lambda\left[\frac{\partial u}{\partial x} + \frac{\partial v}{\partial y}\right].$$

In the above equations, p represents the static pressure, ρ is the density, T is the static temperature, u is the component of velocity in the x-direction, and v is the component of velocity in the y-direction.

The additional equations used to close the system are the equation of state,

$$p = \rho RT,$$

and the total energy per unit volume,

$$e = \rho\varepsilon + \rho\left[\frac{u^2 + v^2}{2}\right],$$

where ε is the internal energy per unit mass, which is related to the static temperature through

$$\varepsilon = C_v T.$$

Sutherland's law,

$$\frac{u}{u_r} = \frac{T_r + 110°K}{T_\infty + 110°K}\left[\frac{T_\infty}{T_r}\right]^{3/2},$$

was used for the viscosity, $\lambda = -(2/3)\mu$, and the Prandtl number was taken to be 0.72. The ratio of specific heats, γ, was set equal to 1.4.

The split predictor-corrector difference method devised by MacCormack (1970) to solve equation (1) was used, and can be defined as follows:

$$\overline{U_{ij}^{n+(1/2)}} = U_{ij}^{n} - \frac{\Delta t}{\Delta y}\left[G_{ij+1}^{n} - G_{ij}^{n}\right], \tag{2a}$$

$$U_{ij}^{n+(1/2)} = \frac{1}{2}\left[U_{ij}^{n} + \overline{U_{ij}^{n+(1/2)}} - \frac{\Delta t}{\Delta y}\left(\overline{G_{ij}^{n+(1/2)}} - \overline{G_{ij-1}^{n+(1/2)}}\right)\right], \tag{2b}$$

$$\overline{U_{ij}^{n+1}} = U_{ij}^{n+(1/2)} - \frac{\Delta t}{\Delta x}\left[F_{i+1j}^{n+(1/2)} - F_{ij}^{n+(1/2)}\right], \tag{3a}$$

and

$$U_{ij}^{n+1} = \frac{1}{2}\left[U_{ij}^{n+(1/2)} + \overline{U^{n+1}} - \frac{\Delta t}{\Delta x}\left(\overline{F_{ij}^{n+1}} - \overline{F_{ij-1}^{n+1}}\right)\right]; \tag{3b}$$

where

$$U_{ij}^{n} = U(i\Delta x,\ i\Delta y,\ n\Delta t),$$

$$F_{ij}^{n} = F(U_{ij}^{n},\ i\Delta x,\ i\Delta y,\ n\Delta t),$$

$$\overline{F_{ij}^{n+1}} = F(\overline{U_{ij}^{n+1}},\ i\Delta x,\ i\Delta y,\ n\Delta t + \Delta t).$$

This essentially consists of two applications of a modified Euler predictor-corrector pair. The first application, equations (2), ignores the x-derivatives in equation (1); whereas, the second ignores the y-derivatives. This numerical computation uses data obtained from data in the $t = t_n$ plane, see figure 1, to advance the solution at x_i, y_i by an amount Δt.

If $L_y(\Delta t)$ is defined as an operator which represents the operations performed in equations (2) and $L_x(\Delta t)$ is the corresponding operator for equations (3), then the solution of equation (1) can be advanced in time, with second-order accuracy, by the following sequence:

$$U_{ij}^{n+2} = L_y(\Delta t)L_x(\Delta t)L_x(\Delta t)L_y(\Delta t)U_{ij}^{n}. \tag{4}$$

Equation (4) holds for $\Delta y = \Delta x$; however, significant advantages result when a modification of this technique is used in problems in which it is desirable to have $\Delta y \neq \Delta x$. In this case, larger time steps and closer matching of the numerical and physical domains of dependence is achieved as follows: The solution of equation (1) is advanced by an amount Δt_x with

$$U_{ij}^{n+1} = \pi^{M/2}L_y(\Delta t_y)L_x(\Delta t_x)\pi^{M/2}L_y(\Delta t_y)U_{ij}^{n},$$

where M is the smallest even integer greater than $\Delta t_x/\Delta t_y$, and $\pi^{M/2}$ denotes $M/2$ products of the L_y operator. For the unequal spatial step sizes, stability considerations require that

$$\Delta t_x \leq \frac{\Delta x}{u + c}$$

and

$$\Delta t_y \leq \frac{\Delta y}{v + c},$$

where u and c are the local velocity and speed of sound, respectively.

A rectangular grid which grows geometrically in both the x- and the y-direction is shown in figure 1, along with the coordinate system. This

Fig. 1

arrangement is ideally suited to the inlet flow problem, which requires a fine mesh in the immediate vicinity of the leading edge but permits a more coarse mesh in the vicinity of the centerline, downstream, and upstream. For the geometric grid, the mesh spacing is given by

$$\Delta x_i = (1 + \eta_x)\Delta x_{i-1} = (1 + \eta_x)^{i-1}\Delta x,$$

and

$$\Delta y_i = (1 + \eta_y)\Delta y_{j-1} = (1 + \eta_y)^{j-1}\Delta y.$$

In general, η_x was not equal to η_y and, in the case of the cascade, the η_x used upstream of the leading edge was not necessarily equal to the η_x used to the right of the leading edge.

The Δx and Δy required for good spatial resolution is estimated by assuming that significant terms in the differential equations are of the same order of magnitude. Consider the transport term $\partial(\rho vu)/\partial y$ and the viscous stress term $\partial[\mu(\partial u/\partial y)]/\partial y$ in the x-momentum equation. Linerization and differencing gives, for $\eta_x = \eta_y = 0$,

$$\frac{\rho u}{2\Delta y}\left[u_{ij+1} - u_{ij-1}\right] \quad \text{and} \quad \frac{u}{(\Delta y)^2}\left[u_{ij+1} - 2u_{ij} + u_{ij-1}\right].$$

If these terms are of the same order of magnitude, then one would expect the coefficients also to be of the same order of magnitude; that is, $\rho v/2\Delta y \simeq u/2(\Delta y)^2$. This condition, when expressed in terms of mesh Reynolds number, $Re_{\Delta y}$, implies

$$Re_{\Delta y} = \frac{\rho v \Delta y}{\mu} \simeq 2,$$

or, upon introducing the Reynolds number, $Re = 2hu_\infty/\nu_\infty$,

$$\frac{\Delta y}{h} \simeq \frac{2u_\infty}{v}\frac{1}{Re},$$

where h is the half-channel width. The results of Gillis and Brandt (1964)

indicate that, for a Reynolds number of 200, $|v/u_\infty| \leq 1/6$, which indicates $\Delta y/h \simeq 0.08$, is sufficient for good spatial resolution at Reynolds numbers at or below 200.

Equating linearized and differenced terms $\partial(\rho u^2)/\partial x$ and $\partial(\rho vu)/\partial u$ from the y-momentum equations yields $\Delta x = (u/v)\Delta y$ or, again using the results of Gillis and Brandt, $\Delta x \simeq 6\Delta y$. In the present calculations, $\Delta y/h$ was 0.036 or less and Δx was fixed at $2\Delta y$, both of which are conservative according to the above estimates for good spatial resolution.

With Δx determined, the number of mesh points to be used from the inlet plane to the downstream exit plane (N) specified, and the distance from the inlet plane to the exit plane (x_e) specified, the geometric scale factor to the right of the inlet plane (η_x) is computed using the equation

$$\frac{x_e}{h} = \frac{\Delta x}{h}\left[\frac{(1+\eta_x)^{N-1} - 1}{\eta_x} - \frac{1}{2}\right].$$

The scale factors to the left of the inlet and in the y-direction are computed using similar formulae. These equations center the smallest cell in the numerical grid (which has dimensions Δx, Δy) on the leading edge.

3. Initial conditions, boundary conditions, and convergence criteria

The initial conditions are essentially that of a uniform flow, which in terms of the present notation, is $u = u_\infty$, $p = p_\infty$, $\rho = \rho_\infty$, and $T = T_\infty$ for all x and y. The posing of boundary conditions in any numerical calculation requires particular attention. This is particularly true in subsonic flow. As noted by Moretti (1969), the boundary of a subsonic computational region with a permeable boundary on which flow variables are held constant is an ill-posed problem. Certainly this is the case for the time-dependent inlet flow. Perturbation waves created in the interior of the flow accumulate at this type

of boundary. Moretti observed this characteristic in Laval nozzle computations, and similar behavior has been observed in the present calculations for the case of the uniform inlet when all flow variables at the inlet plane were held fixed. Thus, it is necessary to permit the boundary conditions to become functions of time without altering the fundamental character of the problem being studied.

First, consider the boundary conditions for the case of uniform entry. The boundary conditions at the inlet plane specify uniform flow and constant density, which in the present notation is $u_{ij} = u_\infty$, $v_{ij} = 0$, and $\rho_{ij} = \rho_\infty$. The numerical computation of Gillis and Brandt (1964) and the analytic work of Van Dyke (1970) indicate that a pressure gradient across the channel inlet plane is required to maintain the prescribed uniform velocity profiles. Therefore, the pressure distribution across the face of the inlet is permitted to adjust by linear extrapolation from the first two interior points to the inlet boundary after each time step. This boundary condition is then written as

$$p_{ij}^{n+1} = p_{2j}^{n} - (p_{3j}^{n} - p_{2j}^{n}) \frac{\Delta x_1}{\Delta x_2} .$$

The inlet temperature distribution is advanced by using the equation of state.

For the boundary conditions at the plate, a fictitious row of cells below the plate were used, together with the reflection technique on u and v. The pressure in the fictitious cell was updated during each time step by using, as the compatibility condition, the y-momentum equation evaluated at the surface

$$\frac{\partial p}{\partial y} = \frac{\mu}{3} \frac{\partial^2 u}{\partial x \partial y} + \frac{\mu}{2T} \frac{\partial v}{\partial y} \frac{\partial T}{\partial y} + \frac{4}{3} \frac{\mu \partial^2 v}{\Delta y^2} .$$

For an adiabatic wall, the complete set of boundary conditions then becomes

$$u_{i1} = -u_{i2}, \quad v_{i1} = -v_{i2}, \quad T_{i1} = T_{i2},$$

and

$$p_{i1} = p_{i2} - \frac{2\mu_w}{3}\frac{u_{i2} - u_{i-1,2}}{\Delta x_{i-1}} - \frac{4\mu_w}{3}\left[\frac{v_{i3} - v_{i2}}{\Delta y_2} - \frac{2v_{i2}}{\Delta y_1}\right].$$

Symmetry boundary conditions were applied on the channel centerline by using mirror cells on either side of the channel centerline.

The downstream boundary values on u, v, and ρ were updated by linear extrapolation from the two upstream points. This is equivalent to forcing $\partial^2 u/\partial x^2 = \partial^2 v/\partial x^2 = \partial^2 \rho/\partial x^2 = 0$. The pressure on this boundary, which was initially uniform, was held fixed at the initial value. The equation of state was again used to update the temperature.

The distance to the parabolic regime as determined for incompressible inlet flow by Gillis and Brandt (1964) was used to determine the approximate location of the downstream boundary. The basic requirement is that the downstream boundary be sufficiently far removed from the inlet to permit the pressure distribution to become essentially uniform across the channel and, therefore, consistent with the specified downstream boundary condition of uniform pressure at the exit plane. In all of the cases presented in this paper, including both the uniform inlet and cascade calculations, the normalized static pressure distribution, $p/\rho_\infty u_\infty^2$, at the first interior plane upstream of the downstream boundary, was uniform to within 1% for the converged solutions.

The boundary conditions for the cascade are the same as those used for the uniform inlet flow, except ahead of the plate where symmetry requires that $v = \partial u/\partial y = \partial p/\partial y = \partial \rho/\partial y = 0$ on the lower boundary. The distance from the cascade inlet to the upstream boundary was located by specifying that the converged pressure distribution ($p/\rho_\infty u_\infty^2$) over the upstream plane be uniform to within 0.5%.

Equation (1), together with the appropriate boundary condition, was solved for the uniform inlet flow and the cascade at various combinations of

Reynolds number and Mach number, M_∞, ranging from 20 to 150 and 0.089 to 0.364, respectively. For both the inlet and the cascade, convergence to the steady-state solution was not monotonic. Rather, exponentially damped sinusoidal oscillations were observed. Disturbances created in the startup process are at least partially reflected at the channel inlet plane and the downstream exit plane and as a result persist in the interior of the flow field until damped by transmission at the boundaries, viscous dissipation, and heat-conduction effects. Although the somewhat arbitrary method used to update the pressure on the upstream boundary precludes precise comparison, the observed frequencies for both the uniform inlet and cascade flows are in rough agreement with the fundamental resonant frequencies of channels which have one end closed the other end open to the atmosphere (Malecki 1969). In addition, the dependence of the rate of dissipation on frequency showed approximate agreement with the analysis of Malecki, which indicates that radiation, viscous dissipation, and dissipation due to heat condution from a closed-end channel are proportional to the square of the resonant frequency. The solutions with $Re = 150$ were assumed to be converged to the steady-state solution when $\Delta p/\rho_\infty u_\infty^2 \leq 0.02$, where Δp is defined as the amplitude of the pressure fluctuation on the flow centerline at the upstream boundary. The $Re = 20$ solutions, which converged considerably faster than the $Re = 150$ cases, were assumed converged when $\Delta p/\rho_\infty u_\infty^2 \leq 0.005$.

The resulting steady-state solutions were checked for conservation of mass at each streamwise station by using the integral form of the continuity equation. As a percentage of the mass inflow at the upstream boundary, the mass loss ranged from 0.2% for the inlet and cascade flow at $Re = 150$ and $Re = 0.089$ to 2.3% for the inlet flow with $Re = 20$ and $M_\infty = 0.364$.

4. Results and Discussion

For the purpose of comparison with the solutions of Gillis and Brandt (1964), the u and v velocity profiles for the uniform inlet with Re = 20 and M_∞ = 0.089 are shown in figures 2 and 3. At this low Mach number, solutions to the incompressible equations of motion provide a reasonable basis for comparison with the inherently compressible results of the present method. The agreement between the two methods is excellent. The physical interpretation of the velocity maxima observed near the inlet plane is discussed by Gillis and Brandt (1964). The u-velocity profile attains the well-known parabolic shape for an incompressible Poiseuille flow at an x/h of approximately 2.5 (not shown) and maintains that shape to the downstream exit plane located at x/h = 11.0. The centerline velocity also reaches the incompressible asymptotic value of 1.5 u_o at x/h = 2.5. The gradual increase in the centerline velocity for x/h = 2.5 is due to the slight compressibility effect which is present even at this low Mach number. As will be shown, at higher inlet Mach numbers, this rate of increase in the centerline velocity is strongly effected and the classical parabolic shape is no longer obtained.

Figs. 2&3

Figure 4 compares the excess pressure drop at the inlet plane with the results of Gillis and Brandt (1964). The excess pressure drop is the pressure drop beyond that which would be present if the flow were a fully developed Poiseuille flow starting at the inlet plane, and is caused by the viscous interaction in the vicinity of the inlet plane. Mathematically, the excess pressure drop at any point (x*, y) is defined by

Fig. 4

$$\frac{\lim_{x\to\infty}\left[p(x^*, y) - \frac{x\partial p(x, y)}{\partial x}\right]}{\rho_0 u_0^2}.$$

In the present study, $\partial p(x, y)/\partial x$ was evaluated numerically by using the specified pressure at the exit plane and the pressure at an upstream point. As with the velocity distribution, the agreement between the two methods is excellent.

The centerline velocity distributions for the case of the uniform inlet at $M_\infty = 0.089$ and $Re = 150$ is compared to the incompressible numerical solution of Gillis and Brandt (1964) and McDonald, Denny, and Mills (1972), and the analytical results of Van Dyke (1970) in figure 5. Figure 6 makes similar comparisons with the analytical solutions obtained by Van Dyke (1970) and the numerical results of Wang and Longwell (1964) (numerical solution of incompressible Navier-Stokes equations) for a cascade with $Re = 150$ and $M_\infty = 0.089$. There is good agreement between the various numerical solutions, and the slight deviation of the analytical results for the uniform inlet flow is discussed by Van Dyke (1970).

Figs. 5 & 6

Velocity and static pressure distribution on the centerline and at the wall of a cascade with a Reynolds number of 20 and a Mach number of 0.36 is presented in figure 7. The behavior of the centerline velocity in this case is dramatically different from that which is observed for the incompressible case. The asymptotic value of $1.5\ u_\infty$ is no longer approached; rather, the strong favorable pressure gradient that is required to maintain the flow also forces a reduction in the gas density. Conservation of mass, in turn, requires that the flow continuously accelerate. As a result, it is not possible to approach the asymptotic Poiseuille type of flow when compressibility effects are present. The flow approaching the leading edge of the plate decelerates monotonically with the pressure approaching, but not quite reaching, the isentropic stagnation pressure at the leading edge. It is interesting to note that the pressure on the centerline in the vicinity of the inlet plane

Fig. 7

is lower on the channel centerline than at $y/h = 0$, but then drops below the wall pressure inside the channel before proceeding toward a condition of uniform pressure, which is reached at an x/h of approximately 2. This behavior is similar in character to the inviscid flow around the forward portion of an airfoil, where the stagnation line static pressure first increases as the flow approaches the stagnation point and then drops below the free-stream pressure as the flow accelerates away from the leading edge. In the present case, the behavior is attributed to the very rapid rate of growth of the boundary layer near the leading edge (Gillis and Brandt 1964), which causes the flow near the plane of the plate to decelerate as the leading edge is approached. This is followed by a gradual reduction in the u-component of velocity as the flow turns to become parallel to the plate, which requires the negative normal pressure gradient observed downstream of the leading edge.

The centerline and wall temperature distributions for this case are shown in figure 8. Although the centerline temperature distribution falls monotonically due to the expansion process, the temperature at $y/h = 0.0$ first increases, recovering to approximately 60% of the isentropic stagnation temperature, before proceeding to fall as the flow moves down the channel. The difference between the adiabatic wall temperature and the centerline temperature increases continuously, as might be expected, due to the increasing local Mach number.

Fig. 8

The effect of the location of the exit plane is also shown in figure 8, where temperature distributions are shown with the downstream boundary at $x/h = 2.67$ and 3.25. Where no discernable difference exists between the two cases, the $x_e/h = 2.67$ results are not plotted. Only the data in the immediate vicinity of the downstream boundary is effected by the boundary location. The velocity and pressure distributions for these two cases were, for the

scale of figure 7, essentially identical, including the data in the vicinity of the exit plane.

Also, for the cascade with Re = 20 and M_∞ = 0.364, the u/u_∞ and v/u_∞ profiles are presented in figures 9 and 10, respectively. The u-velocity profile at the exit plane (x_e/h = 3.25) differs significantly from the classical parabolic profile, in contrast with the incompressible case where the velocity profile is within 1% of being parabolic at x/h = 2.25 (Gillis and Brandt 1964). The local centerline Mach number at the exit plane is 0.94. Attempts to move this boundary further downstream result in numerical instabilities of the type described below.

Figs. 9 & 10

Figure 11 summarizes the results of solutions obtained for a uniform inlet flow at Re = 20 and several Mach numbers. The pronounced effect of increasing Mach number on the flow acceleration is apparent. This compressibility effect is, in fact, present even at the lowest Mach number of 0.089 where the asymptotic incompressible value for the centerline velocity is surpassed at an x/h of 2.5. At the higher inlet Mach numbers, sonic velocities are approached within a few channel widths. It is necessary that the downstream boundary be kept upstream of the point where the flow attempts to go supersonic. If the downstream boundary is moved beyond this sonic point, numerical instability is encountered. This behavior is consistent with the fact that subsonic, viscous, adiabatic flow through a constant area duct can attain, at most, sonic velocity (see for example Shapiro 1953). To increase the duct length beyond this sonic point results in a "choked" flow which moves the sonic point downstream to the duct exit. To achieve this, a reduction in the mass flow rate is necessary, which is not permitted by the present formulation of the boundary conditions at the inlet plane.

Fig. 11

5. Summary

The compressible viscous flow in the inlet region of a straight channel and the flow into a cascade of semi-infinite flat plates has been studied at Reynolds number of 20 and 150 and at Mach numbers ranging from 0.089 to 0.364. The numerical method of MacCormack (1970) is used to solve the governing Navier-Stokes equations utilizing a nonuniform rectangular grid. Sufficient boundary conditions for the solution of the governing equations are prescribed by including the effect of near field subsonic permeable boundaries. These boundary conditions are well-posed in the sense that the pressure on the upstream in-flow boundary is advanced in time such that accurate steady-state solutions are obtained. No attempt is made to relate the time-dependent part of the solutions to any particular physical unsteady flow. To do this for subsonic flow requires knowledge of conditions outside the permeable boundary.

Comparison of the low Mach number uniform inlet and cascade results with the incompressible solutions of previous authors shows excellent agreement and verifies the consistency of the time-dependent boundary conditions on the permeable boundaries and the utility of the nonuniform grid. Results of computations at the higher Mach numbers for both the uniform inlet and the cascade are presented. The extreme sensitivity of the inlet region flow to increasing inlet Mach number is demonstrated by a rapid acceleration of the flow toward the sonic velocity. Solutions are presented in sufficient detail to provide basic test cases for future analytical or numerical methods which include the effect of compressibility on viscous flows in inlet regions.

REFERENCES

BLANKENSHIP, V. D. & CHUNG, P. M. 1967 J. Heat Transf., Trans. ASME 89 Ser. C 281.

BOUSSINESQ, J. 1891 Comptes Rendus 113, 9.

FRIEDMAN, M., GILLIS, J. & LIRON, N. 1968 Appl. Sci. Res. 19, 426.

GILLIS, J. & BRANDT, A. 1964 Air Force European Office of Aerospace Res. Sci. Rep. 63-73 (AD 614915).

GOSMAN, A. D., PUN, W. M., RUNCHAL, A. K., SPALDING, D. B. & WOLFSHTEIN, M. 1969 Heat and Mass Transfer in Recirculating Flows, Academic Press, London & New York.

KAPILA, A. K., LUDFORD, G.S.S. & OLUNLOYO, V.O.S. 1973 J. Fluid Mech. 57, 569.

MACCORMACK, R. W. 1970 Lecture Notes in Physics 8, 151.

MALECKI, I. 1969 Physical Foundations of Technical Acoustics. Pergamon Press.

MCDONALD, J. W., DENNY, V. E. & MILLS, A. F. 1972 Appl. Mech., Trans. ASME 39, 873.

MORETTI, G. 1969 Phys. of Fluids, Supplement II, 13.

MORIHARA, H. & CHENG, R. 1973 J. Computational Physics 11, 550.

SHAPIRO, A. H. 1953 The Dynamics and Thermodynamics of Compressible Fluid Flow. Ronald Press, New York.

SCHLICHTING, H. 1960 Boundary Layer Theory, McGraw-Hill, New York.

TAYLOR, T. D. & NDEFO, E. 1970 Lecture Notes in Physics 8, 356.

VAN DYKE, M. D. 1970 J. Fluid Mech. 44, 813.

WANG, Y. L. & LONGWELL, P. A. 1964 A.I.Ch.E.J. 10, 323.

WILSON, S. 1971 J. Fluid Mech. 46, 787.

Figure Captions

FIGURE 1. Coordinate system, numerical grid, and boundary conditions.

FIGURE 2. Streamwise velocity profiles for uniform inlet at Re = 20, M_∞ = 0.089. ———, full numerical (present method); ○, full numerical (Gillis and Brandt 1964); ×, parabolic profile.

FIGURE 3. Transverse velocity profiles for uniform inlet at Re = 20, M_∞ = 0.089. ———, present method; ○, Gillis and Brandt (1964).

FIGURE 4. Excess pressure drop at inlet plane for uniform inlet at Re = 20 and M_∞ = 0.084. ○, present method; △, Gillis and Brandt (1964).

FIGURE 5. Centerline velocity for uniform inlet at Re = 150. □, present method (M_∞ = 0.089); ———, Van Dyke (1970); ○, Gillis and Brandt (1964); --------, McDonald, Denny, and Mills (1972).

FIGURE 6. Centerline velocity for cascade at Re = 150. ○, present method M_∞ = 0.089; ———, Wang and Longwell (1964) M_∞ = 0; —— - ——, Van Dyke (1970) M_∞ = 0.

FIGURE 7. Cascade pressure and streamwise velocity at Re = 20 and M_∞ = 0.364. □, centerline velocity; △, stagnation line velocity; ○, centerline static pressure; ◇, stagnation line and wall static pressure; ▷, isentropic stagnation pressure.

FIGURE 8. Cascade centerline and wall static temperature distributions at Re = 20 and M_∞ = 0.364. ○, adiabatic wall temperature (x_e/h = 3.25); ◇, adiabatic wall temperature (x_e/h = 2.67); □, centerline temperature (x_e/h = 3.25); △, centerline temperature (x_e/h = 2.67).

FIGURE 9. Streamwise velocity profiles for cascade at Re = 20 and M_∞ = 0.364. ———, present method; --------, parabolic profile.

FIGURE 10. Transverse velocity profiles for cascade at Re = 20 and M_∞ = 0.364.

FIGURE 11. Centerline velocity distributions for uniform inlet with Re = 20. ———, M_∞ = 0.089; --------, M_∞ = 0.196; —— - ——, M_∞ = 0.288; —— -- ——, M_∞ = 0.379.

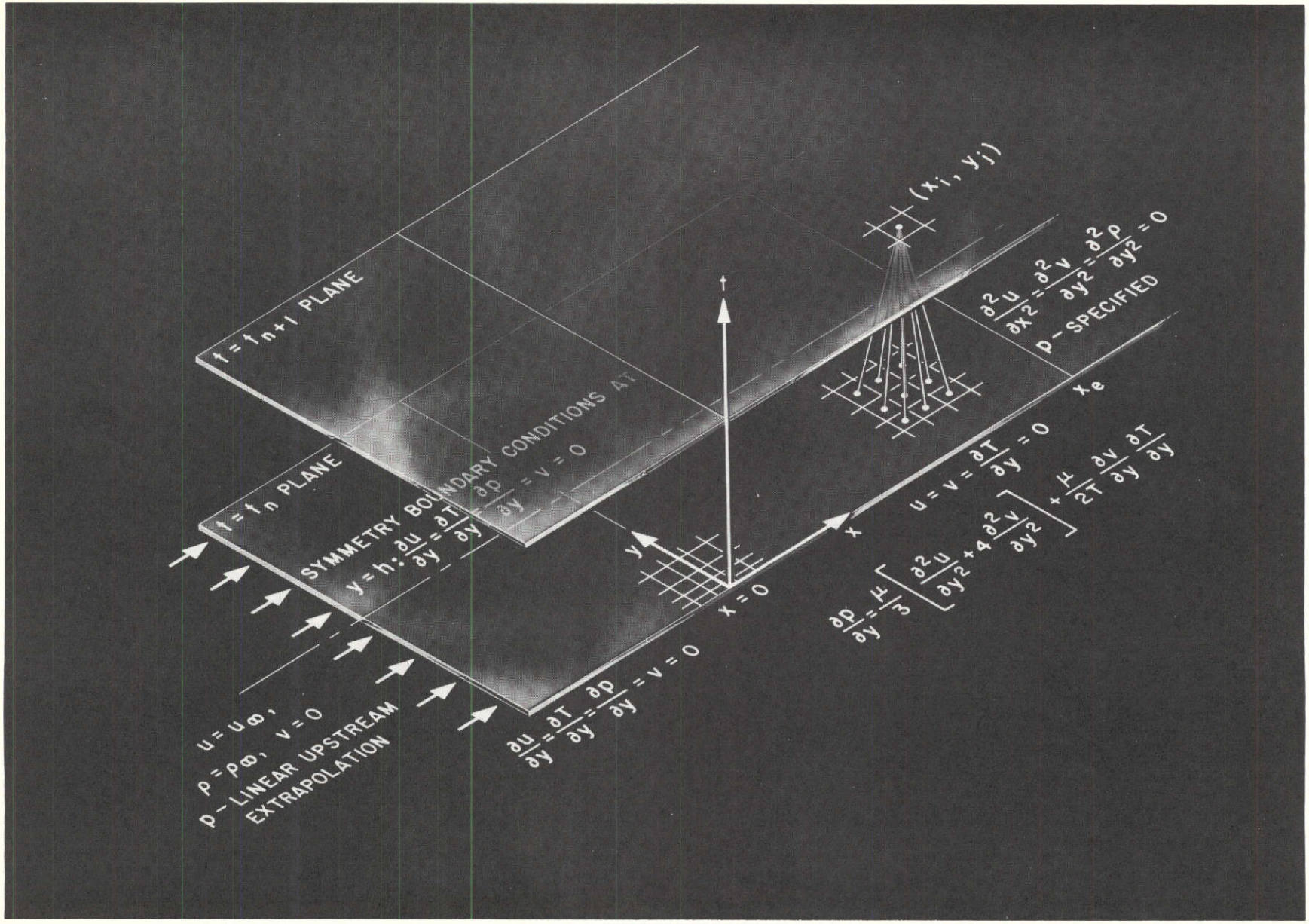
t = tn+1 PLANE
t = tn PLANE
SYMMETRY BOUNDARY CONDITIONS AT
y = h: ∂u/∂y = ∂T/∂y = ∂p/∂y = v = 0
(xi, yj)
∂2u/∂x2 = ∂2v/∂y2 = ∂2p/∂y2 = 0
p - SPECIFIED
t
y
x
x = 0
xe
u = v = ∂T/∂y = 0
∂p/∂y = -μ/3 [∂2u/∂y2 + 4 ∂2v/∂y2] + μ/2T ∂v/∂y ∂T/∂y
∂u/∂y = ∂T/∂y = ∂p/∂y = v = 0
u = u∞,
ρ = ρ∞, v = 0
p - LINEAR UPSTREAM EXTRAPOLATION

Fig. 1

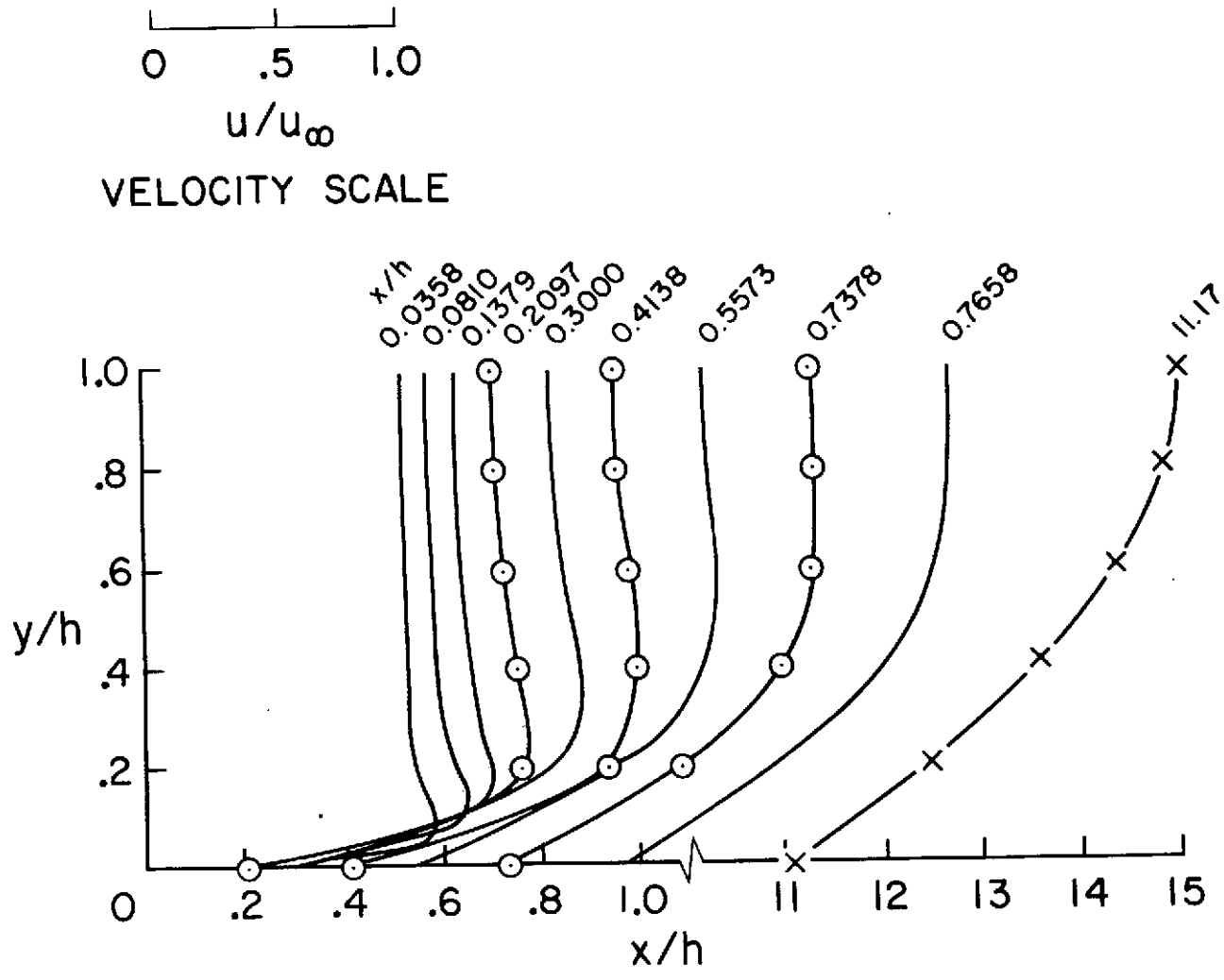
0
.5
1.0
u/u∞
VELOCITY SCALE
x/h
0.0358
0.0810
0.1379
0.2097
0.3000
0.4138
0.5573
0.7378
0.7658
11.17
y/h
1.0
.8
.6
.4
.2
0
.2
.4
.6
.8
1.0
11
12
13
14
15
x/h

Fig. 2

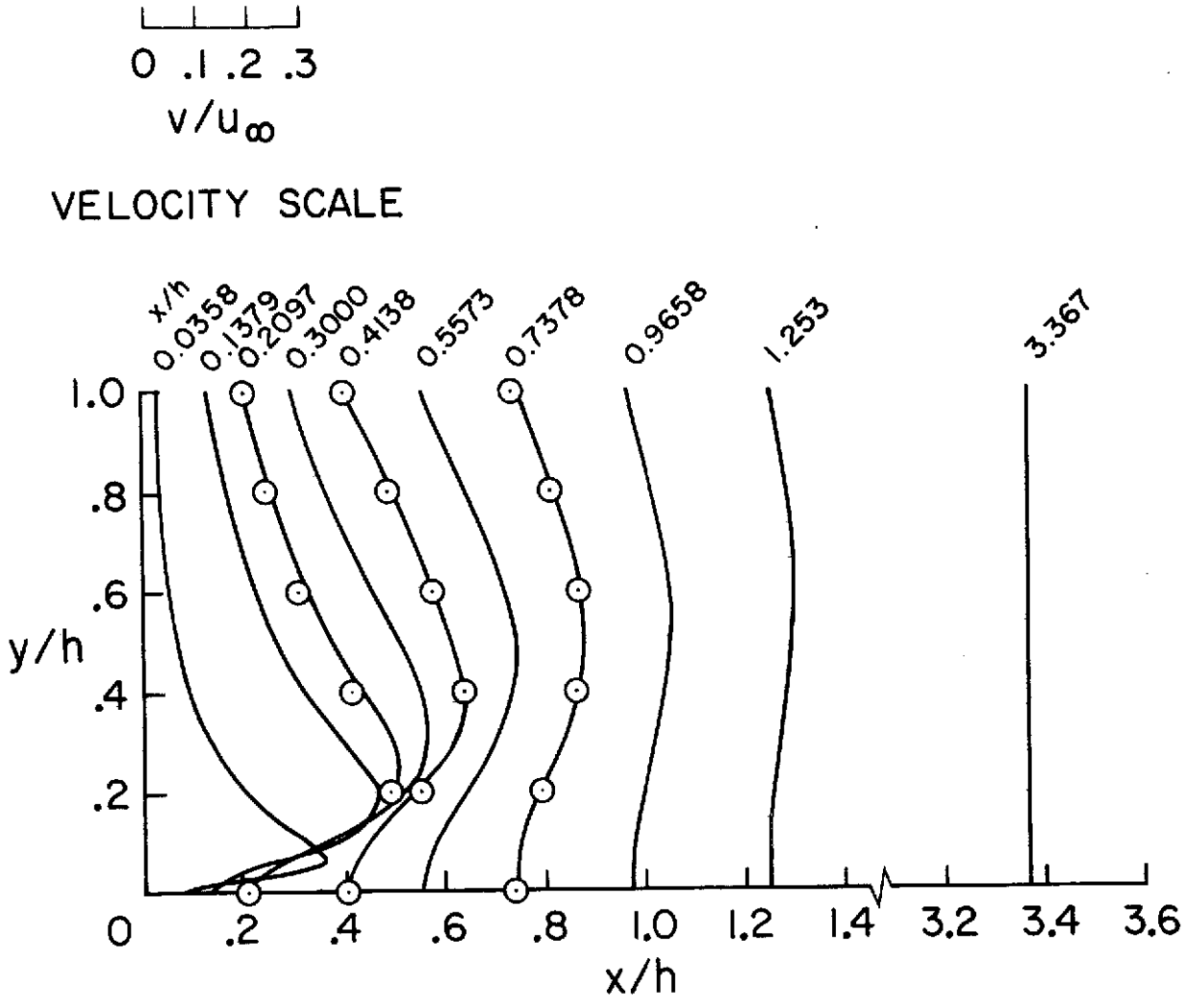
0 .1 .2 .3
v/u∞
VELOCITY SCALE
x/h
0.0358
0.1379
0.2097
0.3000
0.4138
0.5573
0.7378
0.9658
1.253
3.367
1.0
.8
.6
y/h
.4
.2
0
.2
.4
.6
.8
1.0
1.2
1.4
3.2
3.4
3.6
x/h

Fig. 3

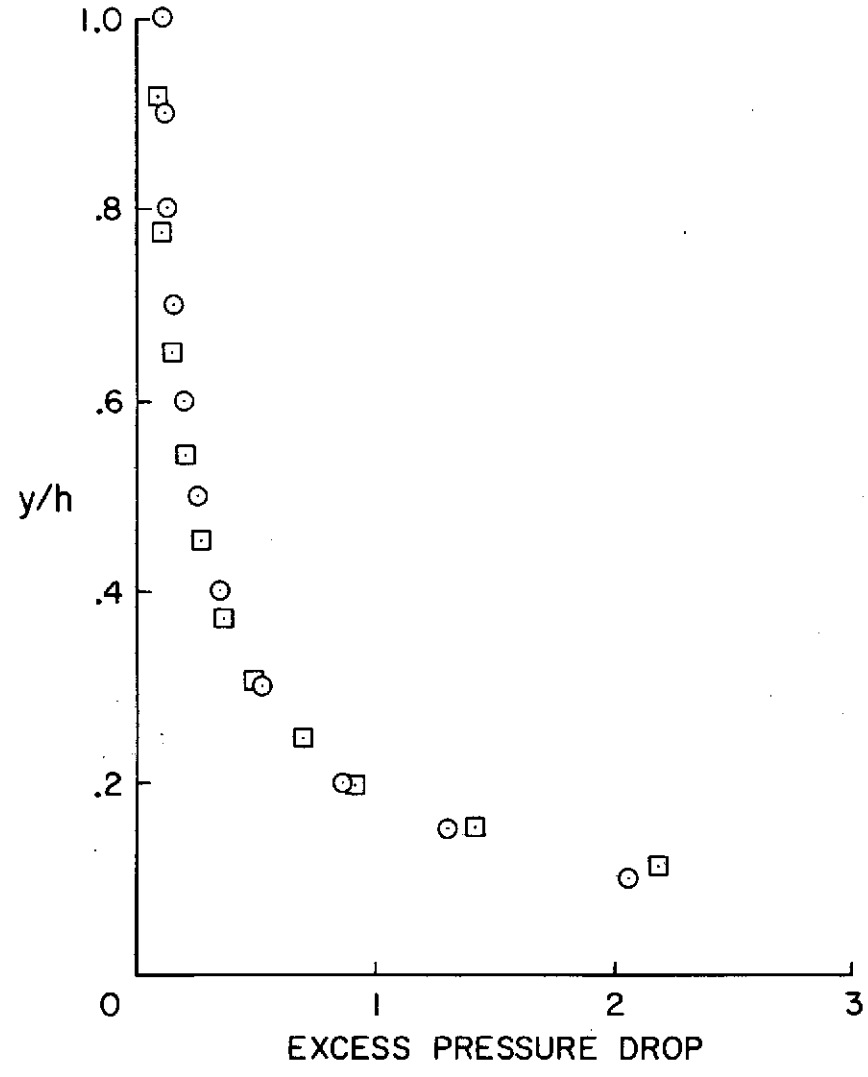

Fig. 4

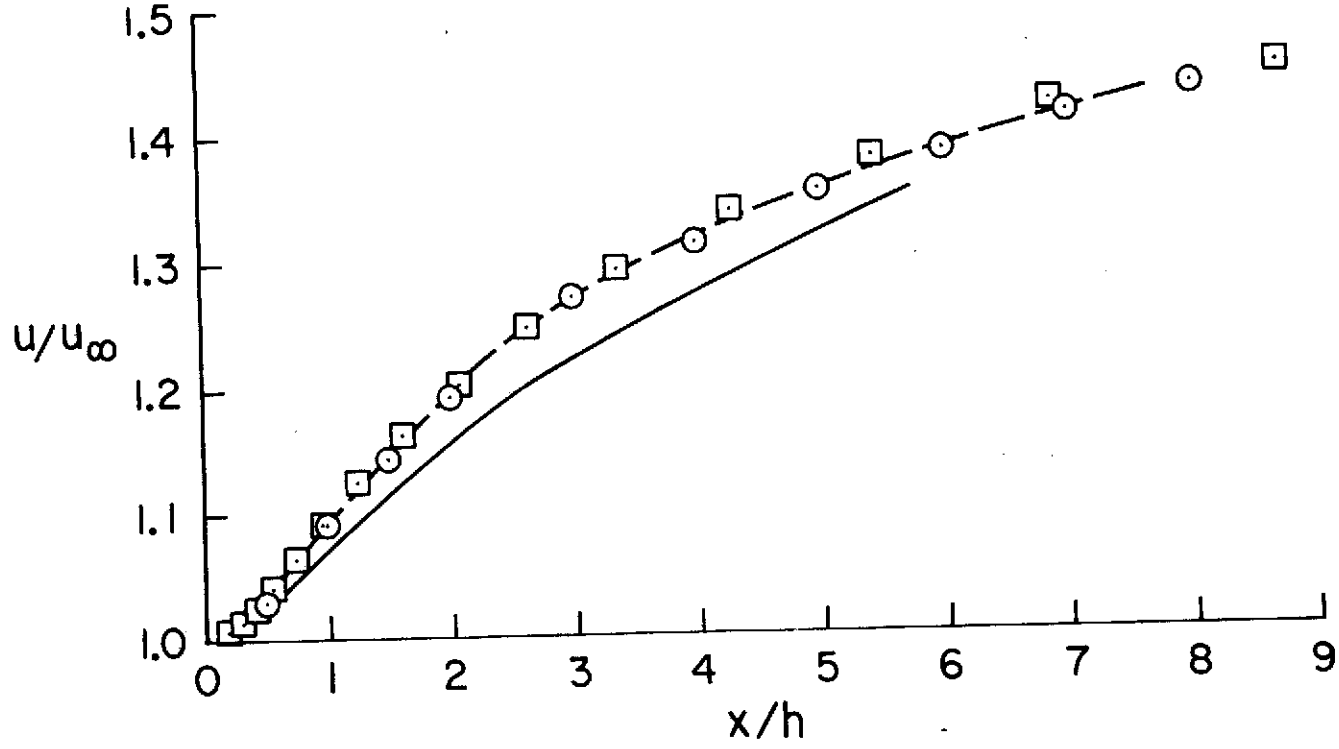

Fig. 5

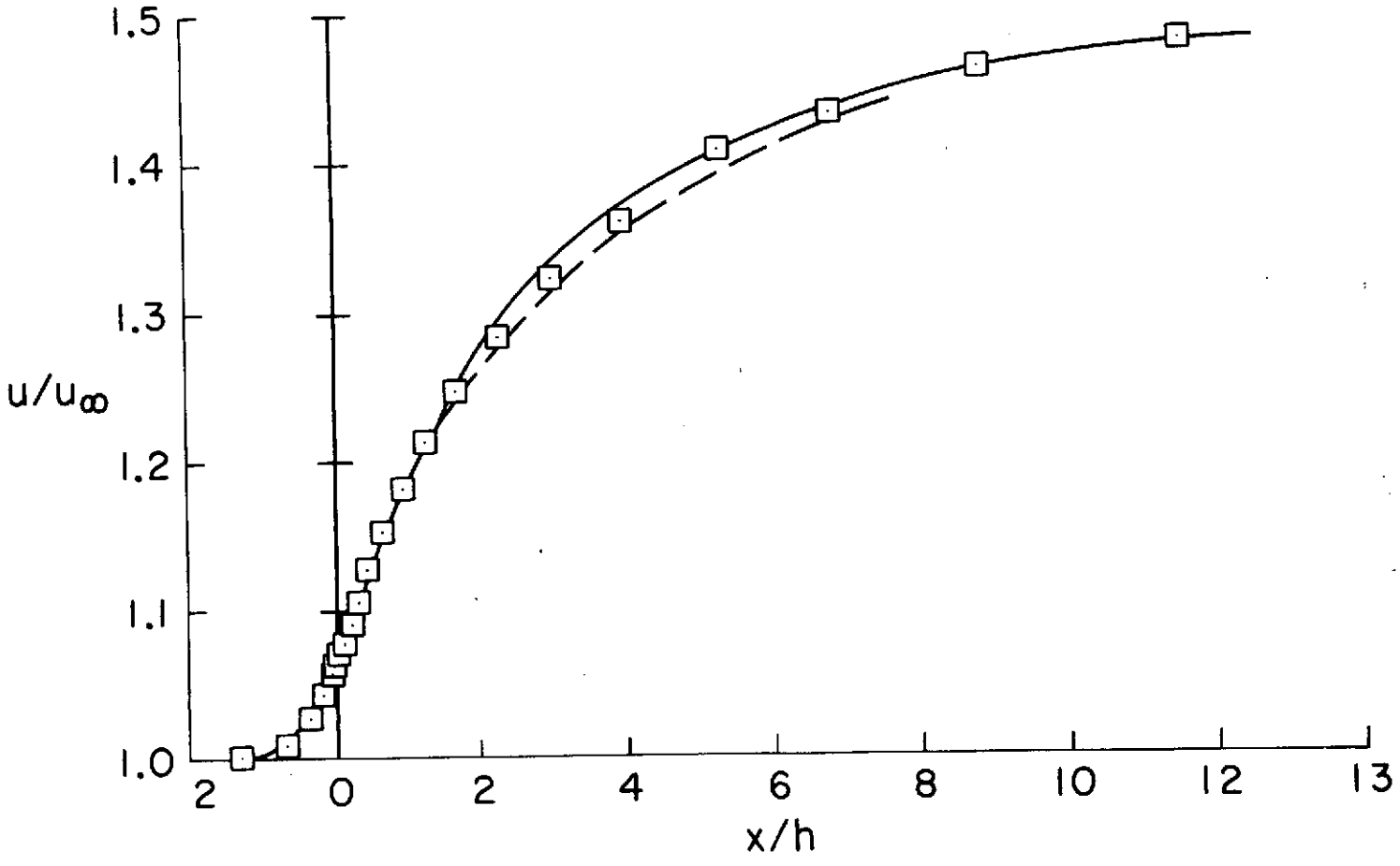

Fig. 6

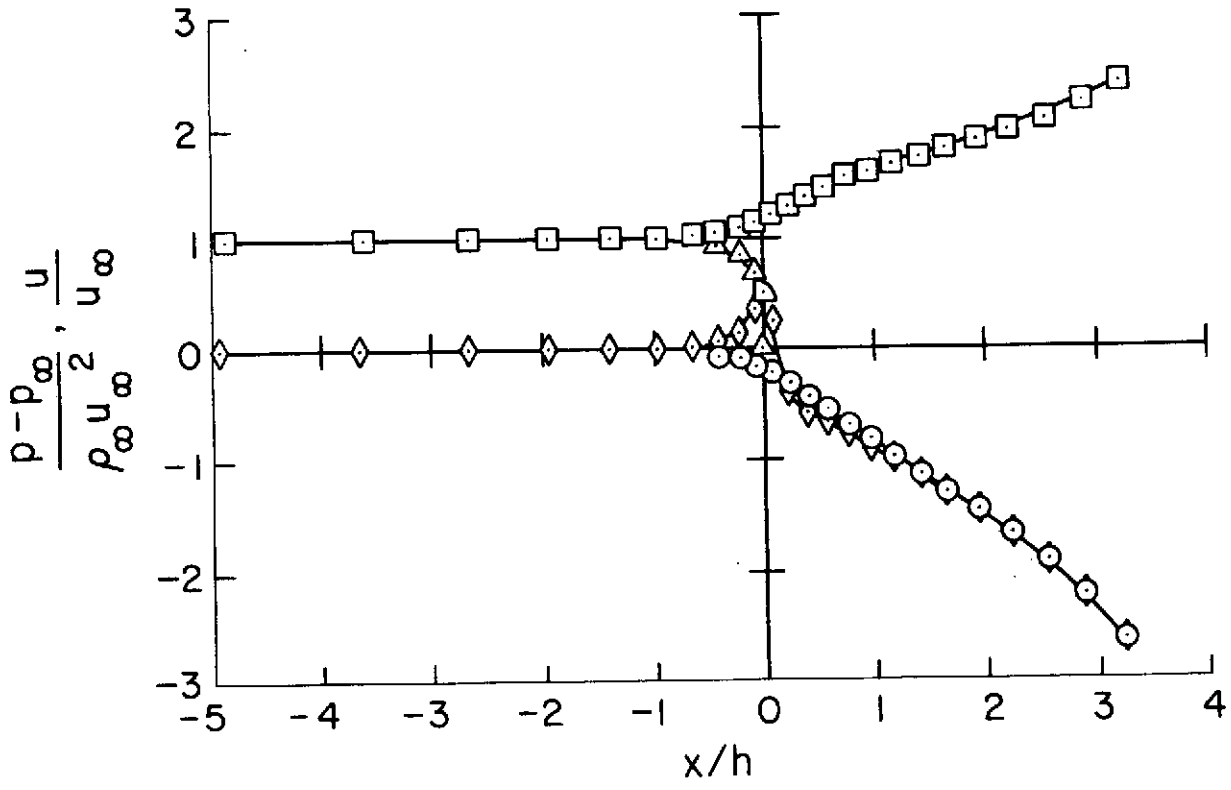
3
2
1
0
-1
-2
-3
-5
-4
-3
-2
-1
0
1
2
3
4
x/h
$\frac{p-p_\infty}{\rho_\infty u_\infty^2}$, $\frac{u}{u_\infty}$

Fig. 7

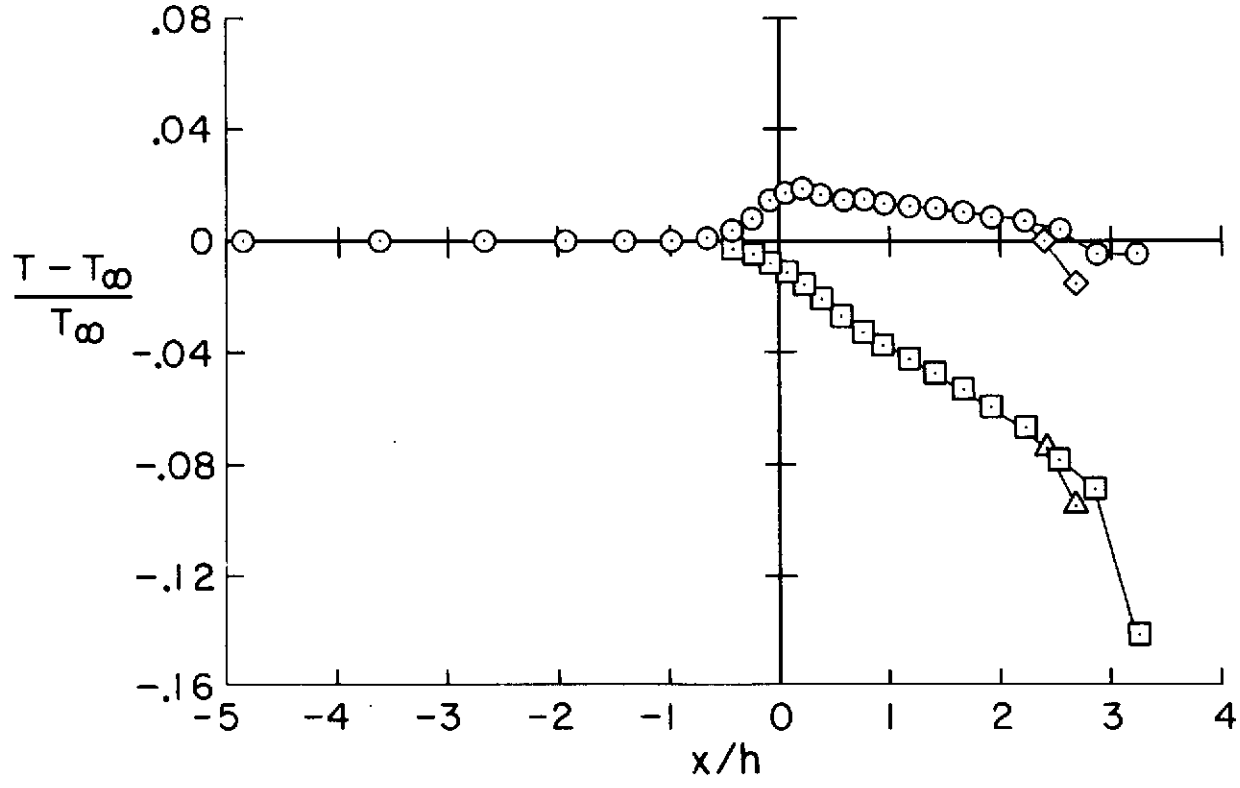

Fig. 8

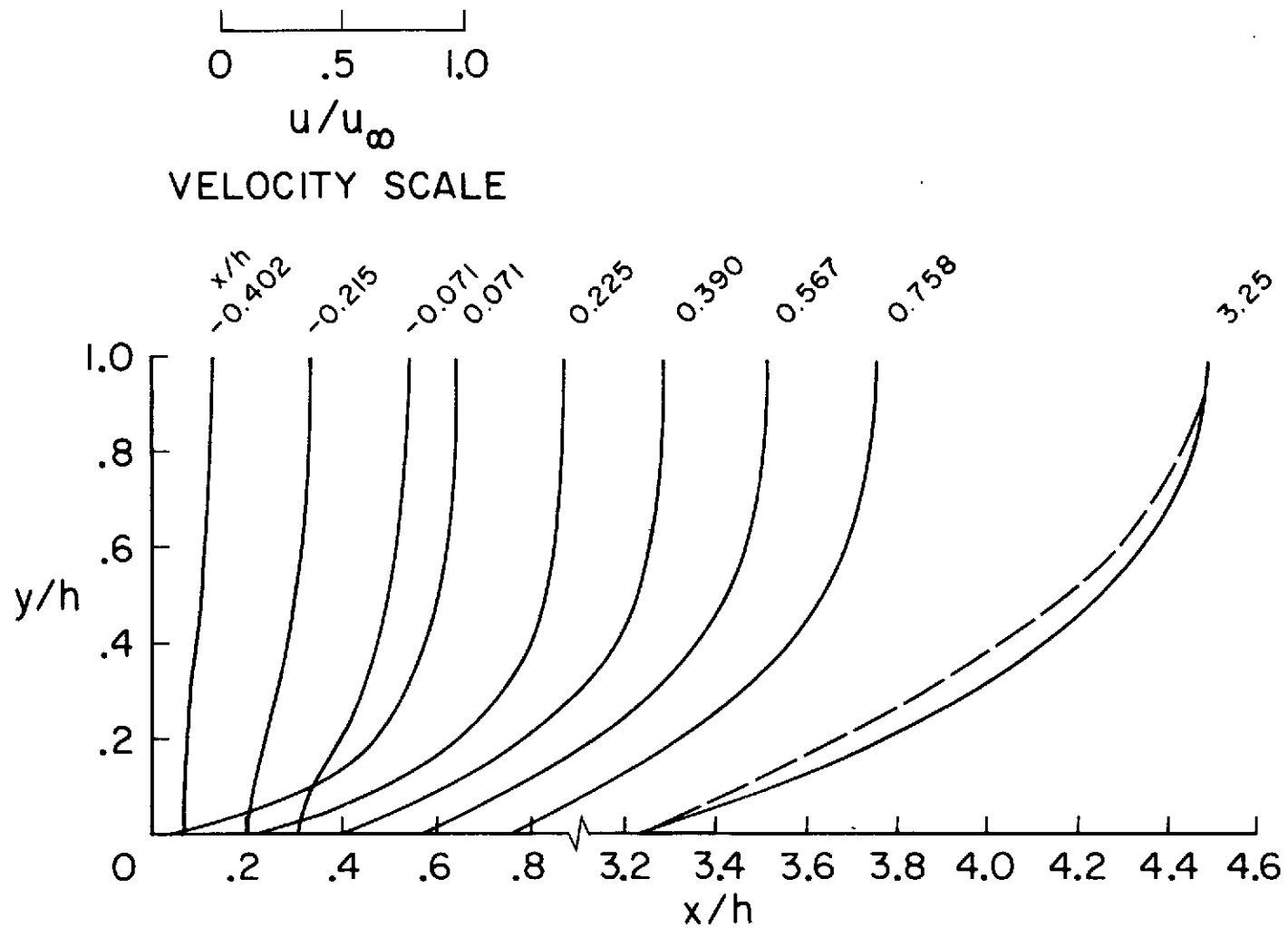
0
.5
1.0
u/u∞
VELOCITY SCALE
x/h
-0.402
-0.215
-0.071
0.071
0.225
0.390
0.567
0.758
3.25
1.0
.8
.6
.4
.2
y/h
0
.2
.4
.6
.8
3.2
3.4
3.6
3.8
4.0
4.2
4.4
4.6
x/h

Fig. 9

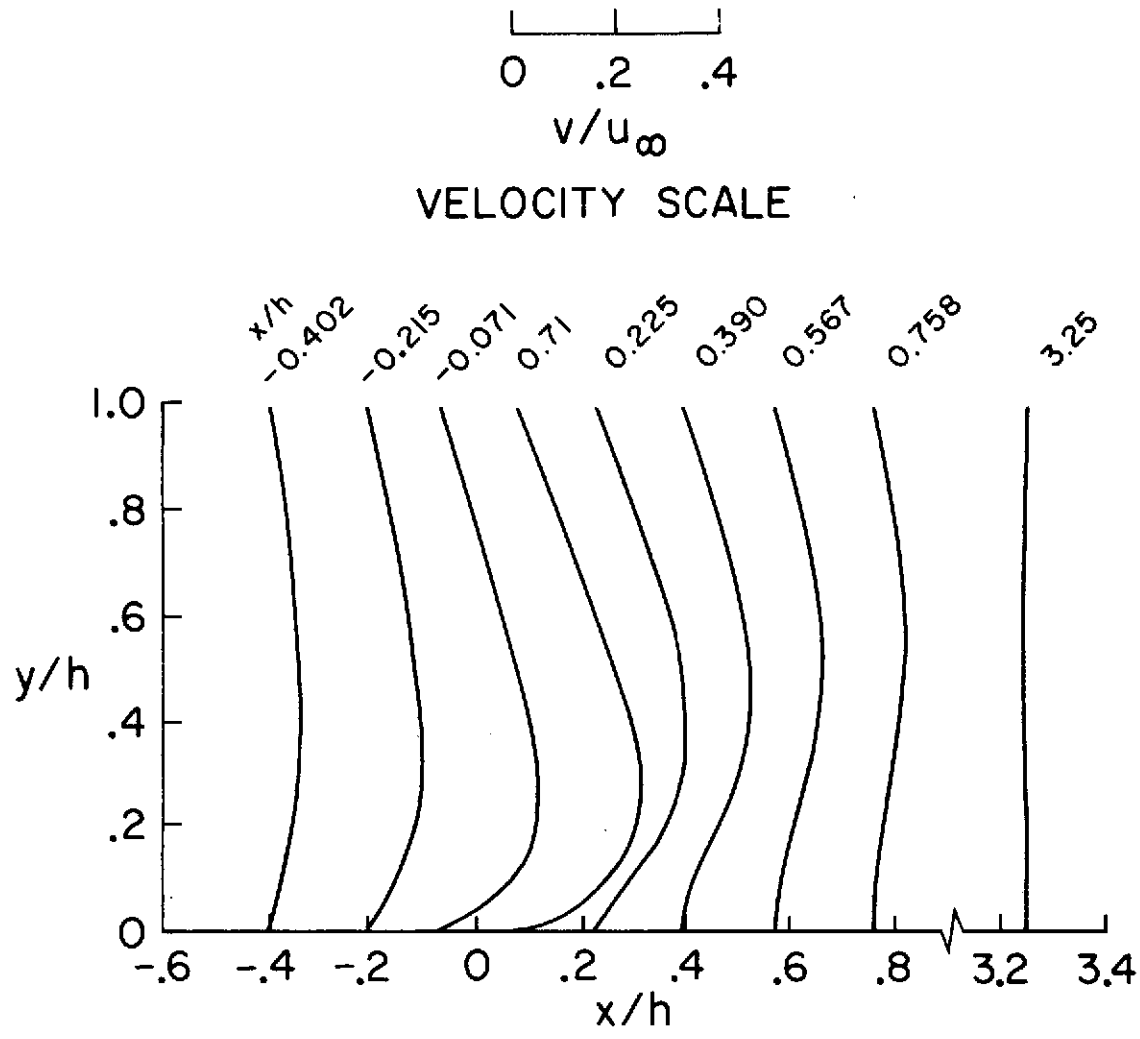
0 .2 .4
v/u∞
VELOCITY SCALE
x/h
-0.402
-0.215
-0.071
0.71
0.225
0.390
0.567
0.758
3.25
1.0
.8
.6
.4
.2
0
y/h
-.6 -.4 -.2 0 .2 .4 .6 .8 3.2 3.4
x/h

Fig. 10

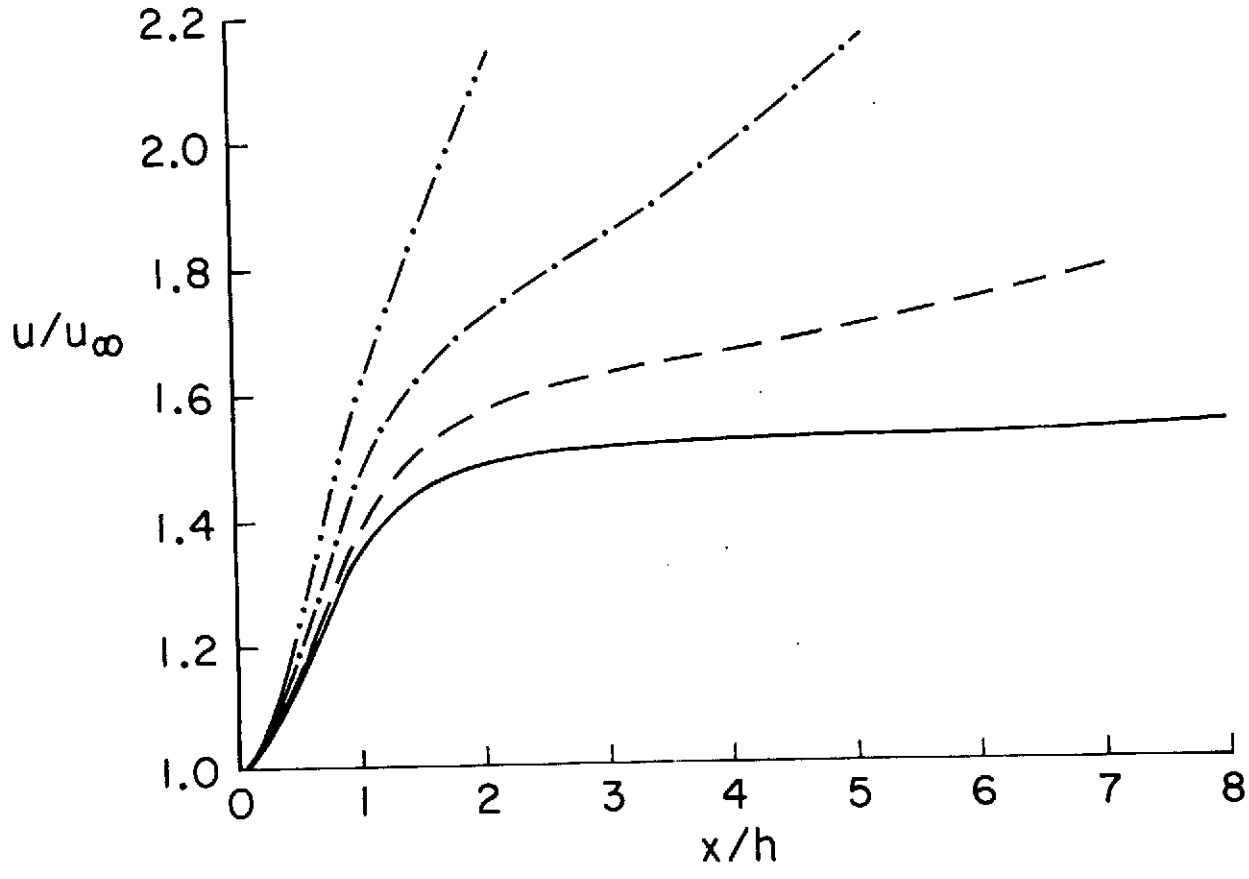

Fig. 11